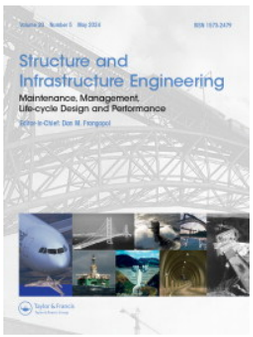

Taylor & Francis
Taylor & Francis Group

Structure and Infrastructure Engineering
Maintenance, Management, Life-Cycle Design and Performance

ISSN: (Print) (Online) Journal homepage: www.tandfonline.com/journals/nsie20

A study of stone arch bridge's flood reliability through a surrogate model approach

Edward A. Baron, Carlos Mendoza Cabanzo, Ana Margarida Bento, Jose C. Matos, Rui Calçada & Kenneth Gavin

To cite this article: Edward A. Baron, Carlos Mendoza Cabanzo, Ana Margarida Bento, Jose C. Matos, Rui Calçada & Kenneth Gavin (26 Feb 2024): A study of stone arch bridge's flood reliability through a surrogate model approach, Structure and Infrastructure Engineering, DOI: 10.1080/15732479.2024.2318648

To link to this article: https://doi.org/10.1080/15732479.2024.2318648

Published online: 26 Feb 2024.

STRUCTURE AND INFRASTRUCTURE ENGINEERING
https://doi.org/10.1080/15732479.2024.2318648

A study of stone arch bridge's flood reliability through a surrogate model approach

Edward A. Baron[a], Carlos Mendoza Cabanzo[a], Ana Margarida Bento[b,c], Jose C. Matos[a], Rui Calçada[d] and Kenneth Gavin[e]

[a]Civil Engineering Department, ISISE, School of Engineering, University of Minho, Guimarães, Portugal; [b]Hydraulics, Water Resources and Environmental Division, Department of Civil Engineering, Faculty of Engineering of the University of Porto, Porto, Portugal; [c]CIIMAR—Interdisciplinary Centre of Marine and Environmental Research, Marine Energy Research Group, Matosinhos, Portugal; [d]Faculty of Engineering, CONSTRUCT, University of Porto, Porto, Portugal; [e]Faculty of Civil Engineering and Geosciences, Delft University of Technology, Delft, The Netherlands

ABSTRACT

Europe's historic masonry arch bridges are culturally and economically significant, but their long-term safety must be ensured. Scour effects are the most common cause of collapse, so it is necessary to carry out structural assessments to mitigate the risk and prevent potential failures. In this study, a metamodel-based method was used to determine the probability of failure of an existing stone arch bridge in Portugal due to local and contraction scour on the abutments. Non-linear finite element analysis supported the calculation of the reliability index, which took into account the soil-structure interaction and the failure mechanism. The variables with the greatest influence on the load-carrying capacity of the structure were identified and a surrogate model was implemented. Fragility curves were then derived based on the surrogate model, using scour depth as a measure of intensity and load factor as an engineering requirement parameter. The results of the study indicate that the load capacity of the numerical model is compromised when the scour depth of 1.5 m reaches the base of the foundation. As a result, stability problems and settlements are observed in the model. At a depth of 2.5 m, the soil reaches its ultimate bearing capacity.

ARTICLE HISTORY
Received 16 February 2023
Revised 15 June 2023
Accepted 5 October 2023

KEYWORDS
Bridge assessment; flood hazard; fragility curves; non-linear structural analysis; scour; soil-structure interaction; surrogate models; uncertainties

1. Introduction

Historic masonry arch bridges are the most typical bridge type in Europe (Olofsson et al., 2005). Due to their economic or cultural importance, it is necessary to ensure their safety, especially against extreme natural events. In recent years, flood damage to bridges has become a significant problem worldwide due to the frequency of its occurrence. Therefore, economic losses and human casualties are the most common consequences (Bento, Gomes, Viseu, Couto, & Pêgo, 2020; Douben, 2006; Yang & Frangopol, 2018). Proske (2018) made a compilation of the main causes of bridge collapses based on studies from around the world. He identified scour as one of the main causes of bridge failure, responsible for more than 40% of collapses recorded in the United States. Xiong, Cai, Zhang, Shi, and Xu (2023) conducted a comprehensive study of hydraulic bridge collapses and found that approximately 50% of these failures were due to hydraulic problems, particularly flooding and scour. Their study included a database of approximately 1700 bridges from the last 200 years.

Comprehensive analyses compiled by recent researchers such as (2007) confirm that bridge failure is primarily due to flooding, making it a significant natural phenomenon with far-reaching consequences. Therefore, there is an urgent need to develop comprehensive safety strategies that prioritize the long-term durability of bridges while meeting the changing needs of current and future users. Current structural reliability methods need to be optimized. Scour can cause costly damage, resulting in compromised safety, service restrictions for bridge users and, in certain circumstances, structural collapse (Lamb, Aspinall, Odbert, & Wagener, 2017). The removal of bed material in the vicinity of bridge foundations has been identified as a cause of numerous bridge collapses worldwide (Brandimarte, Paron, & Di Baldassarre, 2012; Cook, 2014; Melville & Coleman, 2000; Wardhana, Hadipriono, & Asce, 2003). Over a 30-year period, more than 1,000 bridges have collapsed in the United States, 60% of which were due to scour at the bridge foundation (Shirole & Holt, 1991).

Scour effects have been extensively studied by several authors using numerical models, employing different schemes for scour progression and considering different levels of modelling complexity and soil-structure interaction (Tubaldi, Macorini, & Izzuddin, 2018; Zampieri, Zanini, Faleschini, Hofer, & Pellegrino, 2017). In this context, Scozzese, Ragni, Tubaldi, and Gara (2019) highlighted the importance of using three-dimensional models to accurately represent the structural response of masonry arch bridges under the influence of scour-induced effects. Depending on the approach and

CONTACT Edward A. Baron id8033@alunos.uminho.pt

complexity of the problem, different methods can be used to calculate the probability of failure of a structure. One widely used option is stochastic methods, which simplify several aspects of structural behaviour and omit uncertainties in the limit state function. On the other hand, complex methods consider a probabilistic, non-linear structural assessment that takes into account the main uncertainties of the problem. However, the adoption of surrogate modelling techniques in many areas of engineering offers the opportunity to replace traditional models by achieving the desired results and reducing the investment in terms of computational power (i.e. time and effort). For example, Tubaldi, Macorini, and Izzuddin (2020) identified the critical mechanical parameters of masonry arch bridges by considering the associated uncertainties using surrogate models.

Research has been conducted to explore the application of surrogate modelling techniques to streamline the computational process required to define fragility curves (Khandel & Soliman, 2021; Mendoza Cabanzo, Santamaría, Sousa, & Matos, 2022). For this purpose, fragility curves are widely used as they can represent the probability of exceeding a given limit state for a given hazard intensity. Nevertheless, the published literature on fragility functions for bridges exposed to flood hazards is much sparser than for other hazards such as earthquakes (Argyroudis, Mitoulis, Winter, & Kaynia, 2019). Some authors, such as Banerjee and Ganesh Prasad (2013), Dong, Frangopol, and Saydam (2013), and Yilmaz, Banerjee, and Johnson (2018), have investigated the combined effect of flood-related scour and seismic fragility of bridges. However, some studies have developed flood-related fragility curves for concrete bridges with additional requirements such as hydraulic forces, hydrodynamic pressure due to debris accumulation, and deterioration effects due to corrosion (Hung & Yau, 2017; Kim, Sim, Lee, Lee, & Kim, 2017; Ahamed, Duan, & Jo, 2021; Argyroudis & Mitoulis, 2021). Nevertheless, a limited number of publications have addressed the modelling of bridge fragility under the combined effects of flooding and scour, especially in cases with multiple failure modes, using surrogate models (Khandel & Soliman, 2021; Mendoza Cabanzo et al., 2022).

The present research aims to implement a probabilistic-based framework to determine the scour fragility conditions of a masonry arch bridge through a non-linear probabilistic-based analysis using a surrogate modelling approach. The obtained fragility curves will provide valuable insights into the structural response of this particular type of structure to the scour effects on its foundations. Moreover, the proposed structure-soil interaction model uses a three-dimensional analysis to determine the ultimate load capacity. In order to reduce the computational cost associated with this methodology, several strategies are employed, such as a sensitivity analysis to determine the key uncertainty variables and the use of the Kriging metamodel as a mathematical tool to represent the structural behaviour of the bridge.

Following this introduction, Section 2 presents the general aspects of the case study, the bridge over the Leça river. In Section 3, the three-dimensional finite element model is developed, while in Section 4 the scour damage scenarios and the structural behaviour against it are presented. Section 5 presents the reliability analysis using the meta-modeling-based methodology and the obtained fragility curves are presented. Finally, the conclusions of this study are presented in Section 6.

2. The Leça river bridge

2.1. Overall description

The case study consists of a granite stone arch bridge over the Leça river in Ermesinde, Portugal. It is located at PK09 of the Minho railroad line and was built in 1875. The arch bridge has a span of 16 m with a maximum height of 18 m and a total width of 5.31 m. This means that the bridge carries only one track, which consists of monoblock concrete sleepers and UIC60 rails on a layer of variable height ballast. The voussoirs, made of the same material, are approximately one meter thick. As part of the design, four wing walls of granite masonry were proposed to reinforce the bridge abutments. A new pre-stressed concrete bridge with a shallow foundation for a second track on the Minho line was then built next to it. It is important to note, however, that the two bridges were deliberately not structurally connected in order to avoid any adverse effects on the old structure (see Figures 1 and 2).

The Leça railway bridge has been studied and inspected several times in order to maintain its functionality and protect it as a heritage structure. Infraestruturas de Portugal (IP), the Portuguese authority responsible for the preservation of bridges, carried out the last overall inspection at the end of 2020, evaluating the structural components by means of a visual inspection.

Several problems were identified that could affect the long-term durability of the bridge, including: (a) biological fouling on the retaining walls; (b) efflorescence on the deck and arch (caused by lack of drainage); (c) corrosion on the parapets; and (d) cracking in the stone joints. However, the problems identified do not affect the structural performance and are insignificant as deterioration scenarios for the safety assessment.

This case study has been the subject of several studies to characterize its behaviour and structural capacity. The selection of this bridge was driven by several factors. Firstly, it was supported by the iRail program, which focuses on increasing the safety of the European rail network and improving infrastructure. Secondly, the characteristics of the bridge, including its age, type, and foundation (masonry with shallow foundations and a single span), are consistent with the prevailing statistics on the most common railway bridges in Europe (see Figure 3). Finally, the availability of various types of data, such as structural blueprints, dynamic measurements, hydrological data, geotechnical characterization and topographical information for the area, further facilitated the selection.

For example, Arêde et al. (2017) performed an experimental characterization of the bridge materials (granite stone) and masonry joints using core samples and in-situ

Figure 1. Leça railway bridge: (a) upstream view, and (b) downstream view.

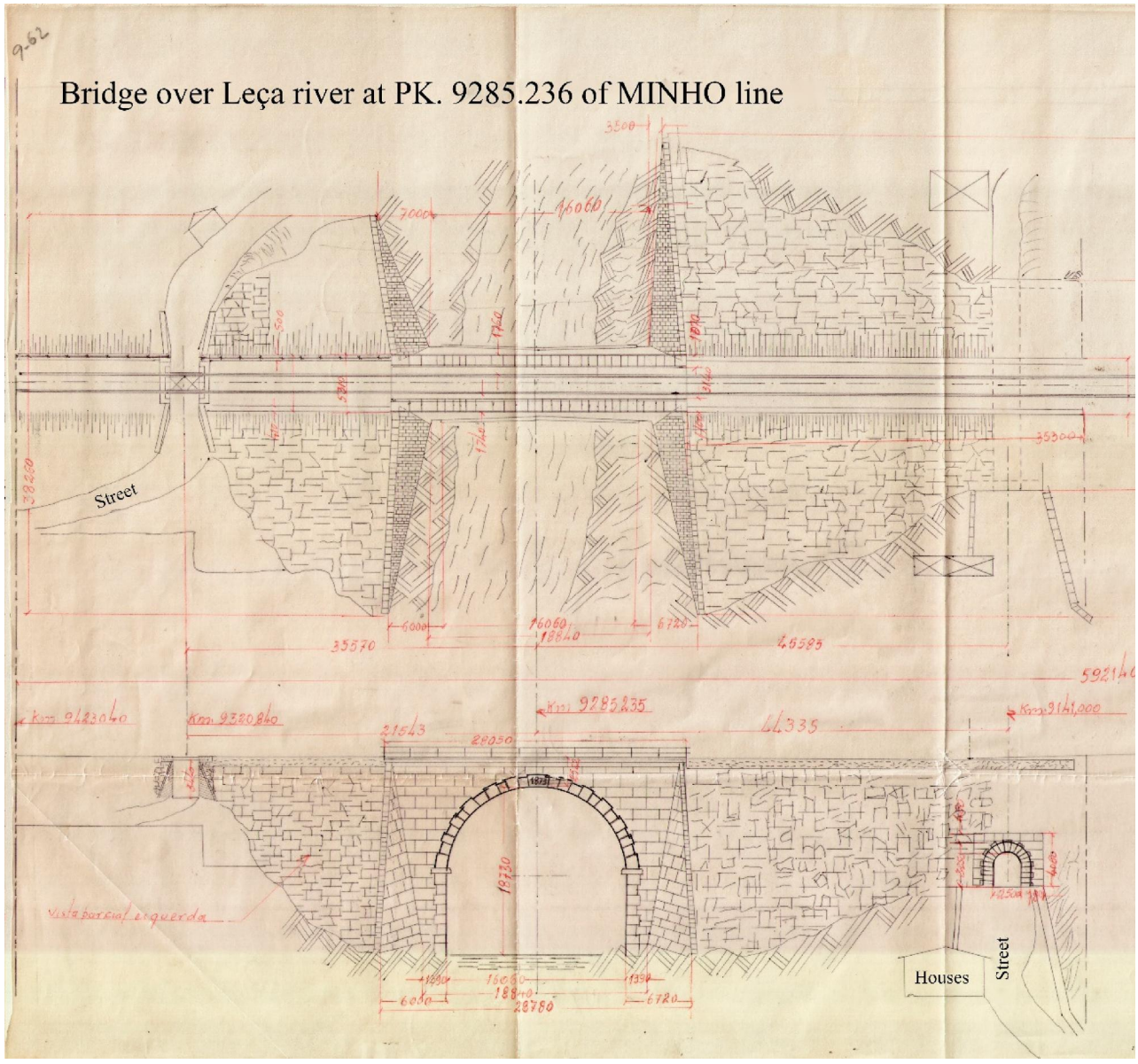

Figure 2. Leça railway bridge original blueprints provided by 'Infraestruturas de Portugal'.

tests on the bridge abutments and arch, which are summarized in Table 1. In addition, Silva, Costa, and Arede (2018) used the experimental results of Arêde et al. (2017) and provided calibrated and validated parameters for the Drucker-Prager model based on the agreement between these data and the numerical simulation results. Consequently, the constitutive model developed in this study was used to analyse and calibrate the finite element model (FEM), as described in previous studies (Costa et al., 2016; Silva, Costa, Arêde, Calçada, & Oliveira, 2019).

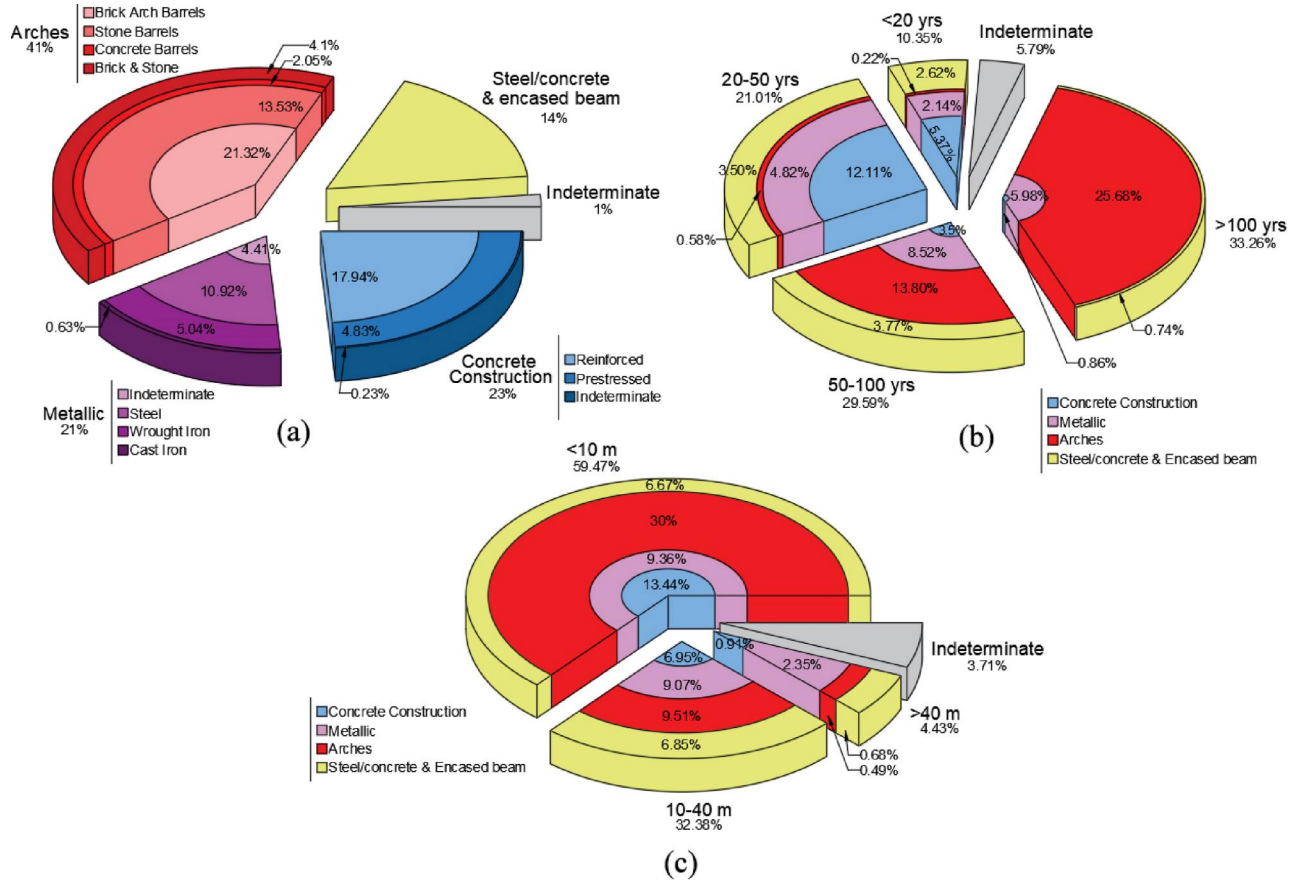

Figure 3. Demography of European railway bridges: (a) types of bridges, (b) age structure of bridges, and (c) bridge span profile. Adapted from (Olofsson et al., 2005).

Table 1. Physical and mechanical parameters of the Leça river bridge stone (Arede et al., 2017).

Parameter	Experimental data (average values)	Test type standard
Unit weight (kN/m^3)	25.2–25.7	–
Compressive strength (MPa)	35.9–81.4	NP EN 12504-1 NP EN 12390-3
Tensile strength by diametrical compression (MPa)	2.3–5.2	NP EN 12390-6
Elastic modulus (GPa)	6.8–10.9	NP EN 14580

With regard to the case study foundation, it was necessary to collect the geotechnical information of the zone. According to the geotechnical information provided by Soares, Araújo, and Gomes (2011), the soil in this sector is mainly composed of Porto granite, with an alteration grade of W_{III} according to the classification proposed by the International Society of Rock Mechanics (ISRM, 1981) and the International Association of Engineering Geology (IAEG) (Dearman, 1995). The IP documentation includes a geotechnical report assessing the condition of the soil. In addition, several Standard Penetration Tests (SPT) and Dynamic Penetration Tests (DPT) were carried out at the locations shown in Figure 4. As a result, the soil profile is drawn and the mechanical properties are defined. The results show that the organic profile is underlain by an alluvium consisting mainly of sandy gravel, a residual soil from the bedrock (see Figure 5).

3. Numerical modelling

3.1. FE model generalities

The methodology described in Baron, Galvão, Docevska, Matos, & Markovski (2023) was used to carry out the safety assessment for the case study. In this sense, a finite element model (FEM) was created to analyse the structural behaviour of the Leça railway bridge. The DIANA FEA software was used in this study to create a three-dimensional model using a quadratic element with eight nodes, based on linear interpolation and Gauss integration. The complete model consists of 122919 elements, 107280 nodes and 6395946 degrees of freedom. From these deformations, DIANA also calculates the strains and Cauchy stresses of each component from these deformations (see Figure 6).

The FEM of the railway bridge is divided into several components (e.g. spandrel walls, arches, abutments, among others), which are modelled using solid elements according to a macro-modelling approach (Lourenço, 2002). The nonlinear behaviour of the granite stone and soil layers was simulated using a constitutive model based on the Drucker-Prager model available in the Diana model library (TNO DIANA, 2016), which takes into account the elastic-plastic behaviour. In addition, the Drucker-Prager model has a yield condition that approximates the Mohr-Coulomb yield surface (conical surface in the principal stress space), while the hardening behaviour is defined as an exponential

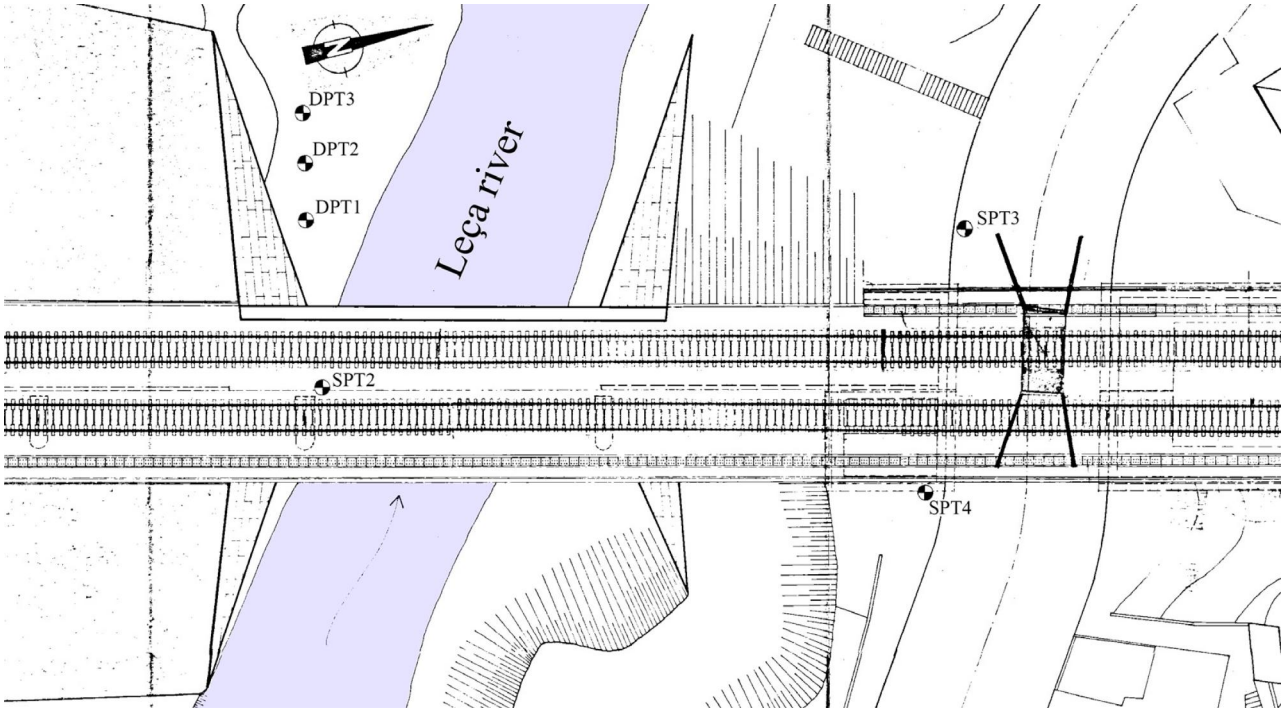

Figure 4. Location of the performed standard and dynamic penetration tests.

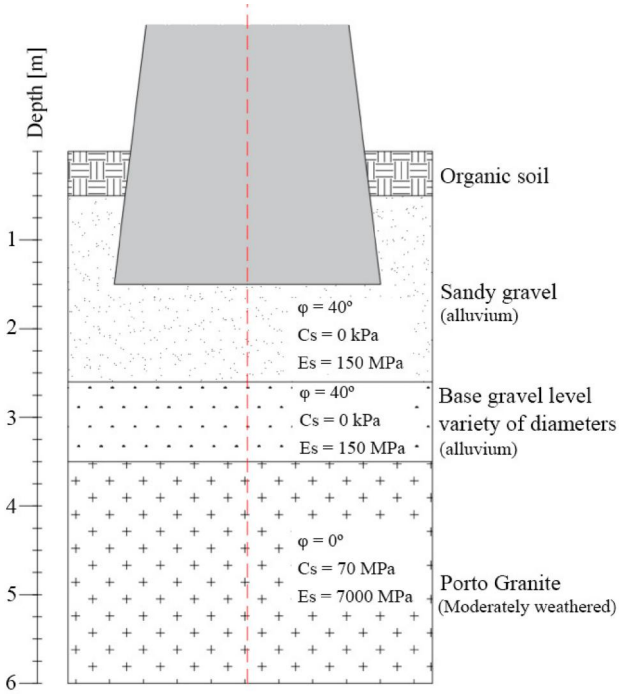

Figure 5. Soil profile of the Leça river bridge abutment.

function (see Figure 7). Symbols in Figure 7 correspond to: κ_{cm} is the plastic strain at uniaxial compressive strength, Ω_{ci} is the compressive relative stress at onset of hardening, Ω_{ci} is the residual compressive relative stress, and G_{fc} is the mode I compression specific fracture energy (area). These values are taken from the ranges given by Silva, Costa, and Arêde (2022).

A variety of load types were used to test the bearing capacity of the case study, including permanent, hydrostatic, and live loads. By using this load configuration, it was possible to assess the performance of the bridge under two different failure mechanisms: i) arch failure due to static bending moment, and ii) soil failure when the maximum bearing capacity is reached. The last type of load used was the LM71 model, proposed by the Eurocode (2003) for the design of railway bridges, which consists of the application of four point loads of 250 kN at a distance of 1.6 m and a uniformly distributed load of 80 kN/m applied at the most unfavourable point, which, according to dos Santos Adrião (2018), is close to 1/4 of the span of the arch; this assumption is maintained after the calculation of the influence line diagram of the case study. Figure 8 shows the characteristic values that apply to the rail tracks, taking into account the regular traffic.

3.2. Boundary conditions

In terms of boundary conditions, rigid supports in the transverse direction were used to simulate the contact with the wing walls. The bridge is constrained in the X direction, which was modelled by constraining all degrees of freedom in the ZY plane of the abutments. The new pre-stressed concrete bridge, it was not modelled as there is no physical connection between the two bridges. However, the reactions of the pre-stressed bridge under dead loads were calculated and implemented in the FEM.

The definition of foundation support and the way it is simulated is not a simple decision. Several studies such as Tubaldi et al. (2022) recommend equivalent idealizations of the soil-structure interaction based on spring models to minimize the computational time and effort of the model. However, in this study, the modelling strategy was defined to be consistent with the scour damage representation presented by Zampieri et al. (2017) and Mendoza Cabanzo

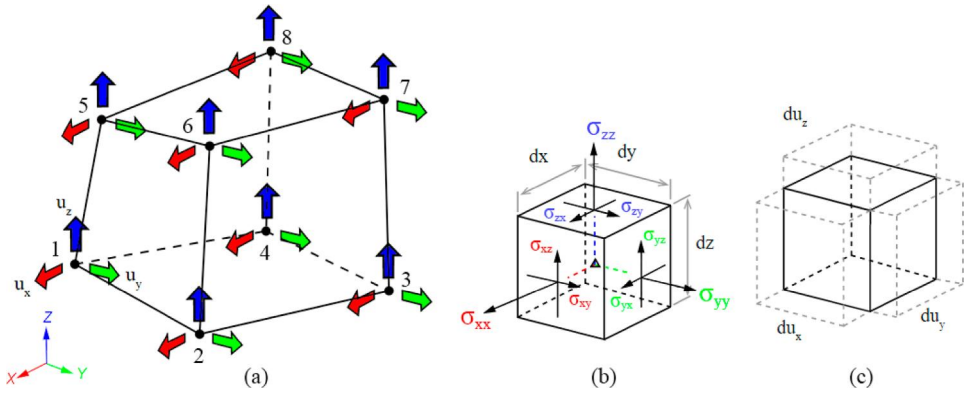

Figure 6. Solid element: (a) displacements, (b) strains and Cauchy stress, and (c) deformation.

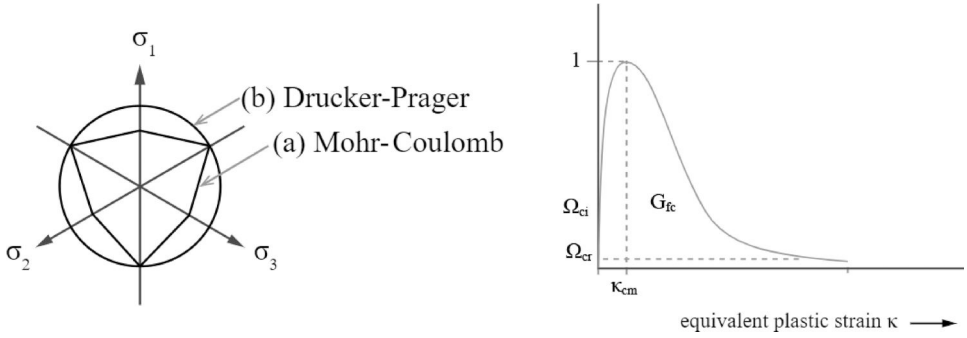

Figure 7. Drucker-Prager yield condition and exponential hardening (TNO DIANA, 2016).

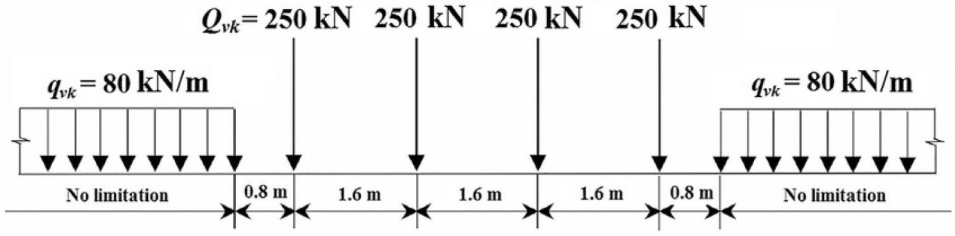

Figure 8. Load model LM71 (European Committee for Standardization, 2003).

et al. (2022). With this in mind, the soil was also represented as a component of the FEM using an eight-node quadratic element. The following assumptions were made for the soil boundary conditions: the Y direction was constrained in the ZX outer layer planes, the X direction was constrained in the ZY outer layer planes, and the Z direction was constrained in the XY bottom plane. Figure 9 displays the graphically the boundary conditions assumed in the FE model.

3.3. Dynamic calibration

As mentioned earlier, all variables that make up an FE model are subject to uncertainty. Nevertheless, deterministic values are traditionally used for the design or analysis of existing structures. Therefore, the FE model parameters need to be calibrated and validated based on experimental data in order to reduce their uncertainty (Costa et al., 2014; Jaishi & Ren, 2005; Ramos, Sena-Cruz, & Ferreira, 2011). In this study, the experimental data from the environmental vibration test recorded by dos Santos Adrião (2018) and the procedure carried out by Costa et al. (2016) and Silva et al. (2022) were used to calibrate and validate the modelled bridge case study. In the experimental test, 14 PCB-393A03 reference piezoelectric accelerometers were used to measure the response, while the identification of the modal parameters was performed using the Enhanced Frequency Domain Decomposition (EFDD) method.

The modal analysis of the bridge was performed by considering the average values of the masonry properties, which were provided by Silva et al. (2019). From the finite element results, the natural frequencies and mode shapes of the first two vibration modes were compared with the experimental results. Figure 10 shows the graphical comparison between the numerical analysis and the experimental test results.

Due to the high value of the error found, the numerical model needs to be calibrated. Consequently, the FEM requires a change in the parameters to reach an acceptable error and the dynamic response is the same as the experimental tests. According to Rangel (2016), the model adjustments are made through the calibration parameters. In this sense, the mass and the stiffness are the variables that

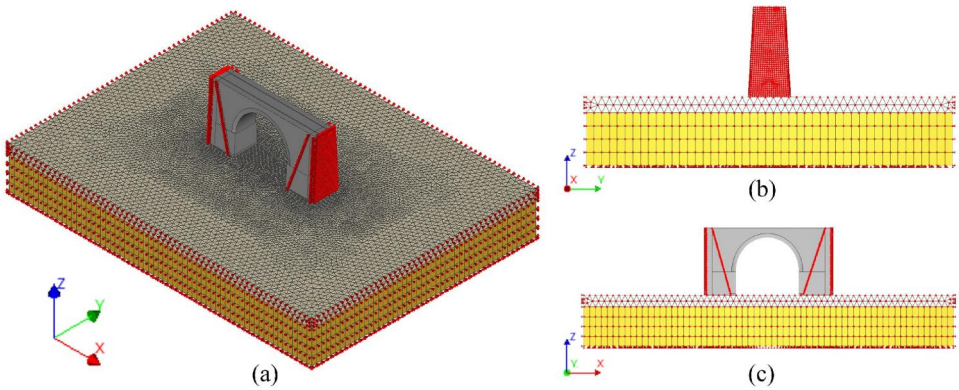

Figure 9. FEM in DIANA software using solid elements: (a) 3D view, (b) lateral view, and (c) front view.

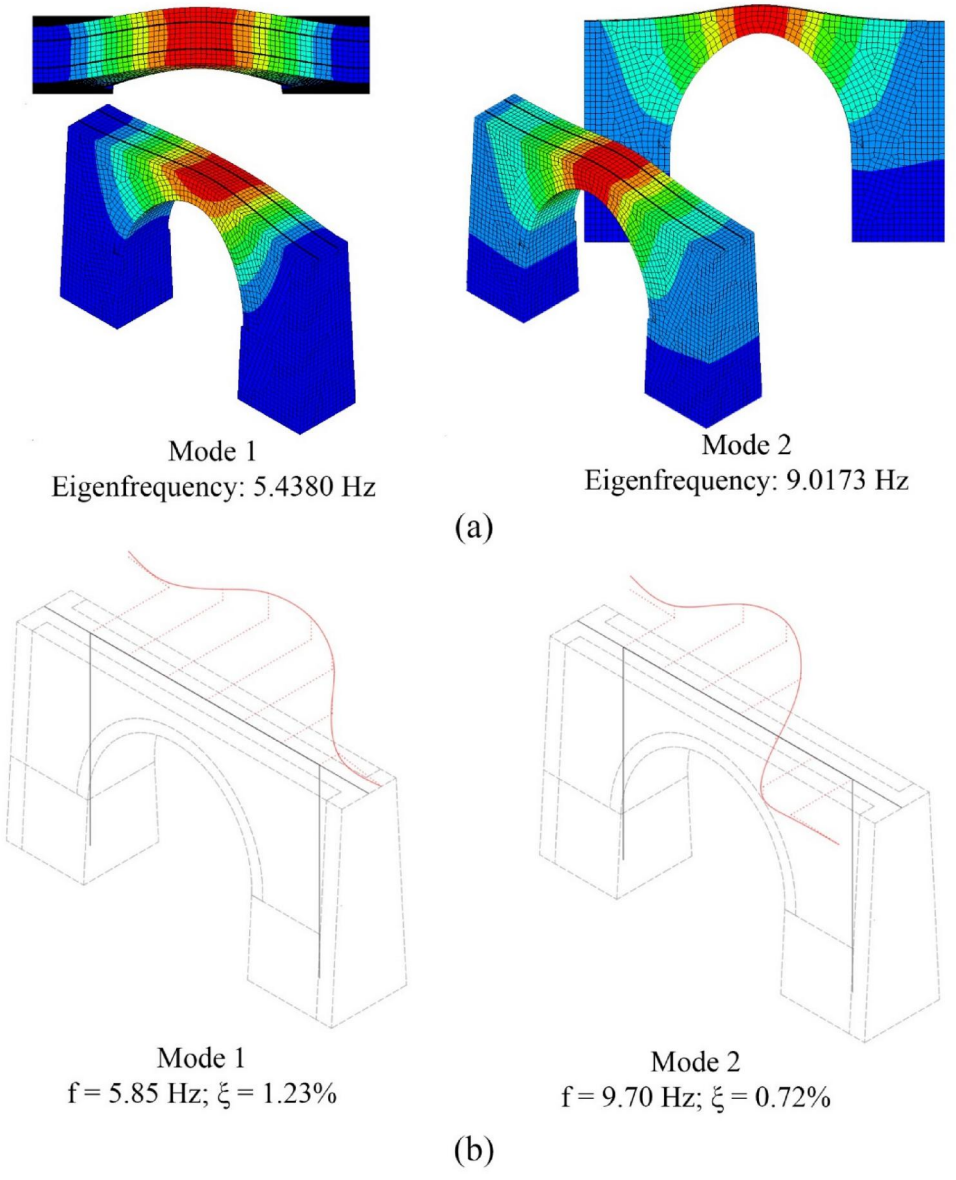

Figure 10. Graphical comparison between dynamic properties: (a) numerical analysis results using DIANA FEA, and (b) experimental test results obtained from (dos Santos Adrião, 2018).

directly affect the dynamics of the structure. Since the modulus of elasticity of the granite masonry is subject to uncertainty, it was chosen as the basis for evaluating the accuracy of the model. Table 2 presents the variation of the masonry elasticity modulus through iterations and the associated percentage relative errors to the experimental data according to Equation (1), where ν_A is the numerical value and ν_E is the experimental value:

Table 2. FE model calibration through modulus of elasticity iteration of granite stone masonry.

	Mode 1 - frequency [Hz]			Mode 2 - frequency [Hz]		
Elasticity modulus [GPa]	Experimental	FEM	Relative Error [%]	Experimental	FEM	Relative Error [%]
Bridge response considering soil modelling						
2.000	5.850	5.438	7.040	9.700	9.017	7.040
2.020	5.850	5.492	6.120	9.700	9.107	6.110
2.110	5.850	5.773	1.310	9.700	9.568	1.360
2.150	5.850	5.871	0.350	9.700	9.729	0.300
Bridge response considering rigid base conditions						
2.000	5.850	5.492	6.120	9.700	9.036	6.850
2.020	5.850	5.512	5.780	9.700	9.077	6.420
2.110	5.850	5.598	4.310	9.700	9.262	4.520
2.150	5.850	5.635	3.680	9.700	9.342	3.690

Table 3. Considered random variables of bridge materials for probabilistic characterization.

Description	Random Variables	Notation	Units	Mean Values	COV (%)	Reference
Granite stone masonry	Modulus of elasticity	E_m	[MPa]	2150	10	(Conde et al., 2021; JCSS, 2006)
	Cohesion	C_m	[MPa]	0.45	15	(Conde et al., 2021; JCSS, 2006)
	Friction angle	F_m	[°]	35.5	10	(Conde et al., 2021; JCSS, 2006)
	Dilatancy angle	D_m	[°]	17.75	10	(Conde et al., 2021; JCSS, 2006)
	Tensile strength	f_t	[Mpa]	2.5	10	(Conde et al., 2021; JCSS, 2006)
Granite stone infill	Modulus of elasticity	E_i	[MPa]	343	10	(Conde et al., 2021; JCSS, 2006)
	Cohesion	C_i	[MPa]	0.45	15	(Conde et al.,2021; JCSS, 2006)
	Friction angle	F_i	[°]	35.5	10	(Conde et al., 2021; JCSS, 2006)
	Dilatancy angle	D_i	[°]	17.75	10	(Conde et al., 2021; JCSS, 2006)
Soil Layer 1 and 2	Modulus of elasticity	$E_{s_{1,2}}$	[MPa]	150	10	(JCSS, 2006)
	Friction angle	$F_{s_{1,2}}$	[°]	40	10	(JCSS, 2006)
Soil Layer 3	Modulus of elasticity	E_{s_3}	[MPa]	7000	10	(JCSS, 2006)
	Cohesion	C_{s_3}	[MPa]	70	15	(JCSS, 2006)

$$\text{RelativeError} = \left|\frac{\nu_A - \nu_E}{\nu_E}\right| \times 100\% \quad (1)$$

Despite the acceptable percentage error obtained for a modulus of elasticity of 2.11 GPa (relative error of less than 5%), a slightly higher modulus of elasticity (with an increase of less than 2%) of 2.15 GPa was chosen for this study because it provides more conservative values (Table 2). This is particularly important as this study only considers the calibration of one parameter, the modulus of elasticity (E). Reducing the discrepancy between the experimental and numerical results by more than 70% (from 2.11 to 2.15 GPa) provides a higher level of confidence for carrying out the sensitivity analysis (the subject of Subsection 3.4).

3.4. Sensitivity analysis

At this stage, a sensitivity analysis was applied to reduce the random variables to be considered in the optimized numerical simulation. The methodology proposed by Matos et al. (2019) allows the identification of the independent variables relevant to the response of the structure under the failure condition. This improves the computational cost of the probabilistic analysis. Therefore, in the sensitivity analysis, the FE model was tested in two different ways: i) physical properties of the bridge materials, considering only the performance of the bridge until failure, and ii) physical properties of the soil and bridge materials, regarding the soil-structure interaction and the maximum bearing capacity of the foundation soil. The random variables were assumed to be independent and characterized by a normal distribution, where the selected means and corresponding covariances (COV) were chosen based on the proposals and experimental results of JCSS (2006) and Conde, Matos, Oliveira, and Riveiro (2021), and are summarized in Table 3.

Figure 11 illustrates the results of applying Equation (2) to the two types of failure criteria to determine the important measure of the random variables:

$$b_k = COV * \sum_{i=1}^{n} \left(\frac{\Delta y_k}{y_m}\right) / \left(\frac{\Delta x_k}{x_m}\right) [\%] \quad (2)$$

The variable b_k refers to the importance measure of parameter k, Δy_k is the change in the output parameter, due to a deviation in the input parameter Δx_k, while the variables x_m and y_m are the average responses and n is the number of parameters generated. In this context, the random variables are tested as $x_m \pm \Delta x_k$ to obtain Δy_k, which, in this case, corresponds to the result of the nonlinear analysis of the FEM, specifically the maximum load factor.

In this analysis, a limit of 20% is considered for the importance measure in order to obtain the variables that have a greater impact on the probabilistic analysis (Matos et al., 2019). For the first scenario, the random variable with the highest importance measure for the response of the bridge failure was the cohesion of the granite stone, as reported in Conde, Ramos, Oliveira, Riveiro, and Solla (2017). For the second scenario, several variables have a direct influence when the soil reaches its maximum bearing capacity. Therefore, the following variables were selected for the probabilistic evaluation: i) modulus of elasticity of the masonry (E_m); ii) cohesion of the masonry granite stone (C_m); iii) modulus of elasticity of the soil layers 1 and 2

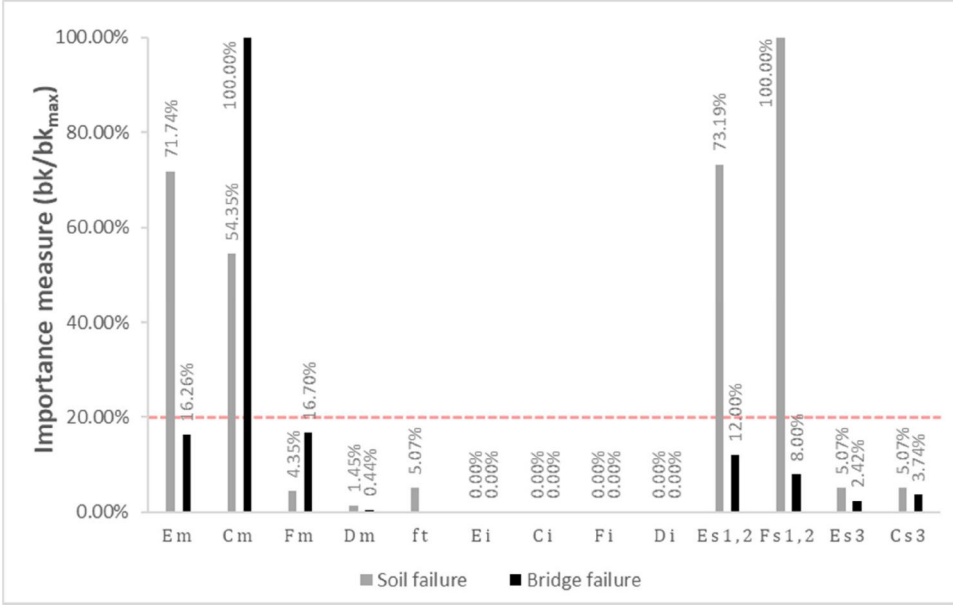

Figure 11. Importance measure for random variables considering failure modes.

($E_{s_{1,2}}$); iv) friction angle of soil layers 1 and 2 ($F_{s_{1,2}}$). The results obtained indicate that the properties of the infill show limited sensitivity, as previously reported in Tubaldi et al. (2020). This observation can be attributed to the application of static loads to the spandrel walls, which are subsequently transferred to the entire structure.

4. Damage scenarios

4.1. Scour profiles

In order to assess the local scour in the abutments, different scenarios were considered, including the location of the scouring process. To achieve this, two scour scenarios were defined to represent the effects of the scouring process on each abutment individually. The scenarios were defined as Scenario 1 (S1) and Scenario 2 (S2) for the effects in the right and left abutments, respectively. Since, the ultimate failure will occur after the soil capacity is reached due to differential settlement in the abutments, a scenario considering scour in both abutments simultaneously was not selected for the probabilistic analysis.

4.2. Scour depth

Scour depth was chosen as the primary measure of intensity due to its significant influence on overall structural behaviour. The results of the hydraulic model presented by Baron, Matos, Calçada, and Gavin (2023) were used to determine the appropriate scour depths for analysis. These results included estimates of scour depths (contraction and local scour) and corresponding flow conditions for different return periods. However, the angle of attack of the flow was not considered due to its low value (< 5%). As a result, several levels of scour were defined in Table 4, ranging from 1.5 m (bottom of the foundation) up to 3.5 m (bedrock).

Table 4. Definition of the damages introduced into the FE model.

Scenario	Scour depth (S_d) [m]	Hydrostatic load (water level) [m]
1	1.0	1.0
2	1.5	1.5
3	1.6	3.5
4	1.7	4.3
5	1.8	5.0
6	1.9	3.79
7	2.0	2.0
8	2.1	1.5
9	2.2	3.7
10	2.5	2.5
11	3.0	3.0

It was then necessary to simulate the effects of extreme floods in the FE model, in order to subsequently develop and test the application of the surrogate model. In this sense, the following damage scenarios were proposed (see Table 4), where the main parameter to be considered was the sum of the scour depth due to the contraction scour caused by the decreasing channel cross-section and the local scour at the abutments. Therefore, these damage scenarios were introduced into the numerical model by removing the soil material under the foundation according to the geometric scour profile recommended by Zampieri, Faleschini, Zanini, and Simoncello (2018), as shown in Figure 12.

Then, for each damage scenario, 100 FE models were defined for each damage scenario considering the selected random variables and generated by Latin Hypercube Sampling (LHS). Therefore, the load-bearing capacity of each generated sample was quantified by performing a non-linear analysis.

4.3. Structural failure mode

Having established the guidelines for the FE model in the previous section, the structure is analysed using a non-linear probabilistic-based analysis that determines the total static load capacity of the structural failure. First, the undamaged structure is analysed to determine the maximum structural

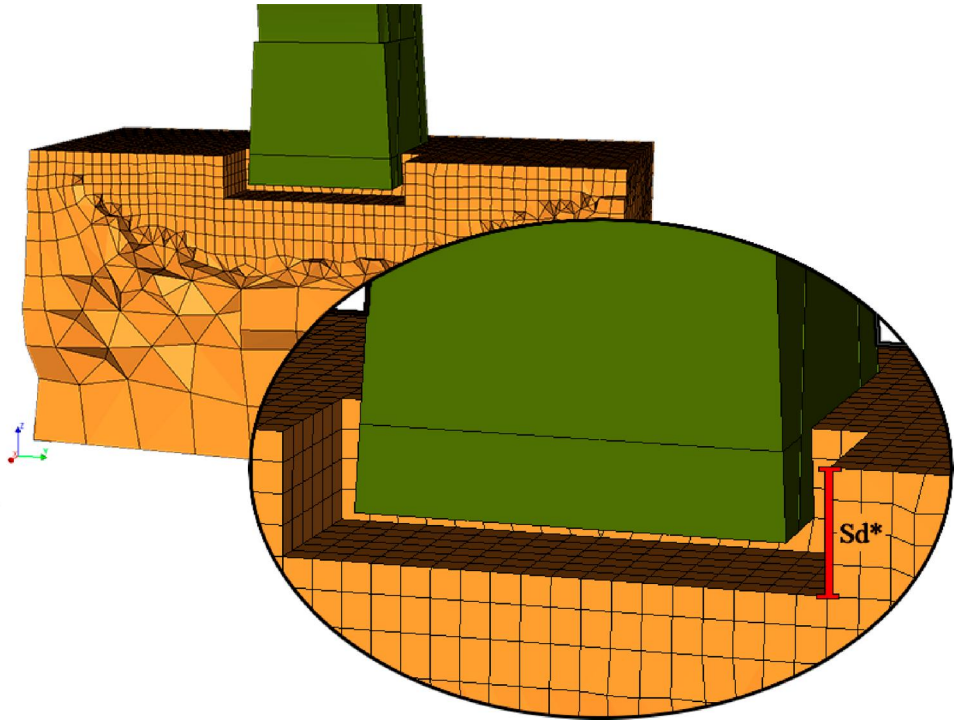

Figure 12. Scour depth (*Sd*) modelling strategy.

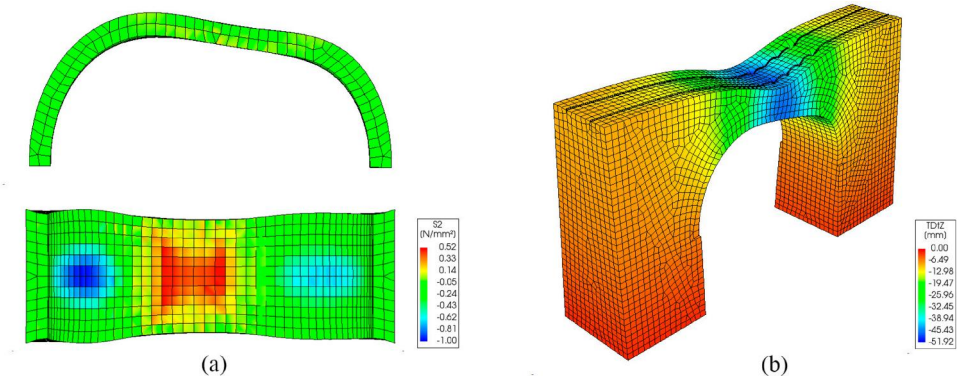

Figure 13. Structural behavior under incremental static load: (a) stress located in the arch; and (b) 3D graphic of global displacements.

capacity (see Figure 13). After a load factor of 12, the arch and spandrel walls enter a state of plasticity. Failure occurs in the arch due to a plastic hinge near the loading zone.

The damage scenarios are then applied step by step to analyse the behaviour of the bridge with respect to the instabilities caused by the lack of soil. In this sense, after reaching a depth of 1.5 m (assuming that the foundation is buried at this total depth), crack patterns are observed in the piers, the base of the foundation, the spandrel walls and the arch, with the last two elements increasing in size (compared to the undamaged model). However, the failure mode remains the same when a lower static load is applied. Figure 14 depicts the crack example assuming a scour in the left abutment at a depth of 2.0 m.

4.4. Soil failure mode

For the second failure mechanism considered, the ultimate bearing capacity of the soil (R_d) in its undamaged form was investigated. In addition, the design contact stress (σ) for the shallow foundation was set at a value of 470 kPa, defined by the ratio F/A_{eff}, where F is the applied vertical force and A_{eff} is the effective area of the foundation. The vertical bearing capacity of the foundation soil was checked using the inequality $\sigma \leq R_d/SF$, where SF is a safety factor, which in this case took the value 1. Consequently, the theoretical R_d (the bearing capacity of the foundation) was estimated by applying the formulation based on the theory of J. Brinch—Hansen (Hansen, 1970), which takes into account factors of the foundation such as the bearing capacity, the geometry of the foundation (shape, depth, slope) and the slope of the terrain. However, the configuration of the soil layers (weaker soil under stronger soil) requires the definition of the failure mechanism.

According to Yang, Zheng, Zhao, and Tan (2016), the failure area depends on the ratio (h/b), where h is the thickness of the weaker soil and b is half the width of the footing (see Figure 15). As this ratio is less than 1, the failure

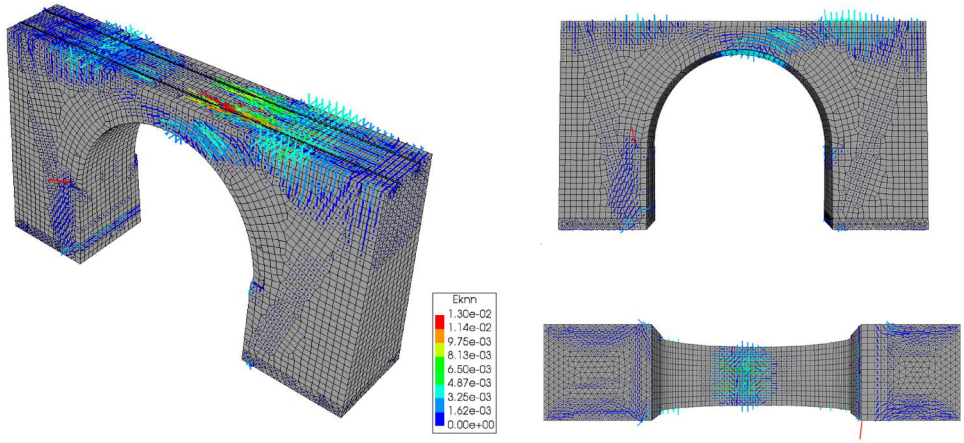

Figure 14. Crack strains obtained from the FE model ($S_f = 2$ *m*).

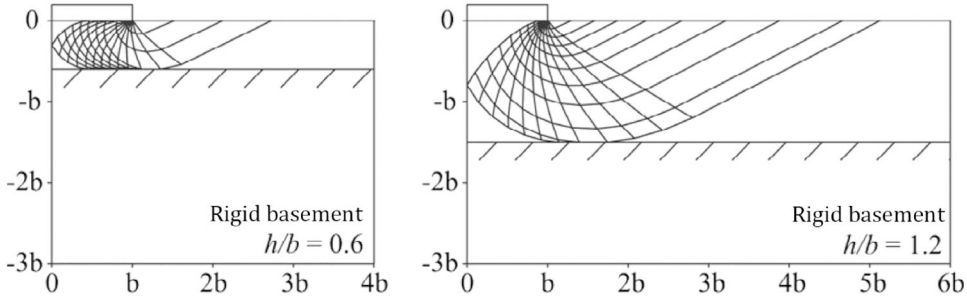

Figure 15. Failure mechanisms considering a weaker soil underlined by a stronger soil, for different values h/b (adopted from F. Yang et al., 2016).

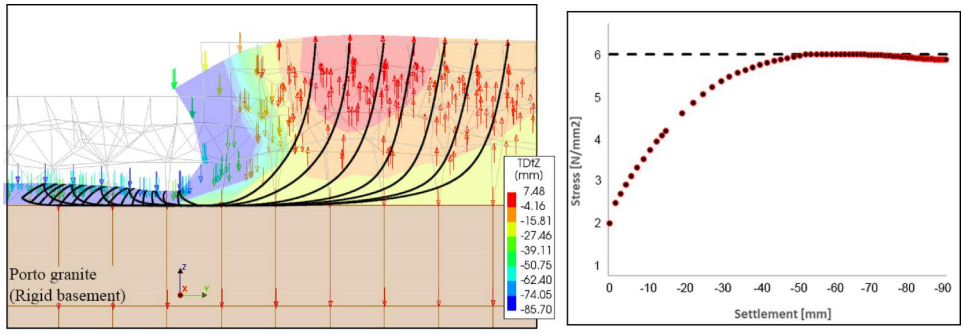

Figure 16. (a) Soil failure surface following J. Brinch – Hansen theory. (b) Stress vs settlement plot.

surface is entirely in the weaker soil layer. Therefore, the theoretical R_d was estimated using the parameters of the weaker soil, and a value of 6050 kPa was obtained.

In addition, the bearing capacity of the soil was calculated using the FE model by testing the soil material by applying an incremental pressure as a result of the non-linear analysis of the arch bridge. Different load cases were investigated to determine the vertical displacement of the soil (z-direction). Figure 16a shows the contour plot of TDtz for a load factor of 5.95 of the applied pressure (1 MPa). In particular, a region of soil was observed where all points had similar vertical displacements. The plot of the total displacement provided visual information about the failure mechanism of the soil. In this sense, it was possible to identify the failure surfaces in the soil. The first region (in blue) represents the vertical movement of the soil with the footing. The second area (in green) is under rotation and is also called the radial shear zone. Finally, the third region (in red) is pushed towards the top and is known as the passive Rankine zone.

To determine the bearing capacity of the soil, the elements were placed at the surface of the soil with the highest stress. As expected, the soil reached its maximum bearing capacity at $q_u \approx 6000$ kPa, which was used as the criterion for determining soil failure. This failure mechanism was therefore considered when the scour depth in the abutment exceeded 2.5 m. Figure 16b illustrates the plot obtained showing the evolution of the highest stress point in the soil model with respect to the corresponding displacement.

5. Reliability analysis

5.1. Surrogate model

Kriging metamodels combined with subset simulation (AK-SS) were used to describe the non-linear limit state function (Guimarães, Matos, & Henriques, 2018) and successfully applied to evaluate the reliability and fragility of arch bridges under scour scenarios (Mendoza Cabanzo et al., 2022). Subsequently, a Kriging surrogate model was created using UQlab and validated based on previously defined random variables. The surrogate model uses a universal trend type, an anisotropic ellipsoidal Matérn 5/2 correlation function that defines the Gaussian process and the cross-validation estimation method (Marelli & Sudret, 2014). The leave one out method was used to validate the surrogate model. The surrogate model was trained based on the load factors (i.e. output parameters) obtained from the evaluation of the numerical model based on an experimental design of 100 samples of the variables obtained from the sensitivity analysis (i.e. input parameters).

The Latin Hypercube Sampling (LHS) method was used to obtain the experimental design for each one of the scour levels (i.e. scour depth values in Table 4). In general, 80% of the samples in the experimental design were used to train the metamodel and 20% were used for validation. In addition, the standard error of the mean was used as a stopping criterion when a value of less than 1% of the mean was reached. Using the surrogate model and the relevant variables, an experimental design with 10000 simulations was evaluated using the Monte Carlo (MC) sampling method to estimate the capacity curve (Guimarães et al., 2018). It was then fitted with the probability distribution function (i.e. GEV, Gumbel, and Kernel) based on the generated histogram of adequacy factors (i.e. the number of load increments that the structure can withstand without collapsing, based on the applied load), allowing the definition of the resistance curve R. Figure 17 shows the process for the results related to the S1 scenario.

The previously determined characterization of the resistance of the structural system is directly related to the applied live load. In this sense, it results from the maximum load factor applied to the LM71 model. The resistance curve is thus multiplied by the mean value of the PDF describing the live load, with its COV depending on the random variables affecting the resistance. Therefore, the mean value of the loading PDF should be defined as a unitary loading factor. In addition, the load curve follows a Gumbel distribution with a unitary mean, since the resistance curve was obtained as a factor of the applied traffic load, namely the LM71 model from the Eurocode (2003). The associated COV was 15%, as recommended by Matos et al. (2019). Nevertheless, the uncertainty associated with the traffic loads should be determined by monitoring data.

The reliability of the structure was evaluated using Equation (3), which represents the limit state function. The variable G was introduced into UQlab using the probabilistic distribution of the load curve S and the resistance curve R:

$$G = R - S \tag{3}$$

In addition, model uncertainties for limit state models (defined by a Gaussian distribution with a mean of 1 and a COV of 15%) were considered based on the model code recommendations of the Joint Committee on Structural Safety (2006) for the stability of shallow foundations with homogeneous soil profiles. To obtain the structural reliability index for a given discharge value, conventional methods such as MC may require numerous simulations to converge to a satisfactory level of accuracy. Therefore, subset simulation techniques were used here to overcome such limitations by solving simpler reliability problems with intermediate threshold values (Au & Beck, 2001). Upon completion of the reliability analysis, the probability of failure and reliability index were determined for each scour depth value (see Figure 18).

Figure 19 presents the reliability index obtained for both scenarios, S1 and S2, representing scour in the right and left abutments, respectively. The different points represent the values of the reliability index obtained for each level of scour (ranging from 0 m to 3 m depth). As expected, the reliability index decreases with increasing scour depth. Finally, comparing the target reliability (i.e. $\beta_{target} = 4.3$, which corresponds to a failure probability of less than 10^{-5}) for structures with high human and economic losses according to NP 1990 (2009), it can be concluded that the structure may not be within the safety levels when faced with severe scour conditions (i.e. when reaching below the foundation).

5.2. Fragility analysis

A fragility function typically correlates a given hazard, represented by an intensity measure, with the expected physical damage (e.g. collapse) using the exceedance probability. They are also useful because they provide the ability to introduce uncertainty in both capacity and demand while determining the reliability of a structure over a range of loads, typically represented by a lognormal distribution (Argyroudis et al., 2019). Flood-related fragility curves can also support quality control strategies before, during, and after a flood event (Khandel & Soliman, 2021).

A lognormal fit was performed on the fragility curve to the previously determined failure probabilities. A script was used to obtain the coefficients based on the generalized linear model (Nelder & Wedderburn, 1972). For this application, the generalized linear regression model was used, in which the response (dependent variable) is expressed as a linear function of all the predictors (independent variables), as described in Nelder and Wedderburn (1972).

Figure 20 illustrates the fragility curve fitted to a lognormal distribution, where it can be observed that the probability of failure due to the traffic load increases with increasing scour depth. As expected, it was found that for scour profiles where the scour depth does not erode the soil below the foundation base, the effect on the structural response is small and the slight decrease in the reliability index of the masonry arch bridge is negligible (Mendoza Cabanzo et al., 2022; Zampieri et al., 2017).

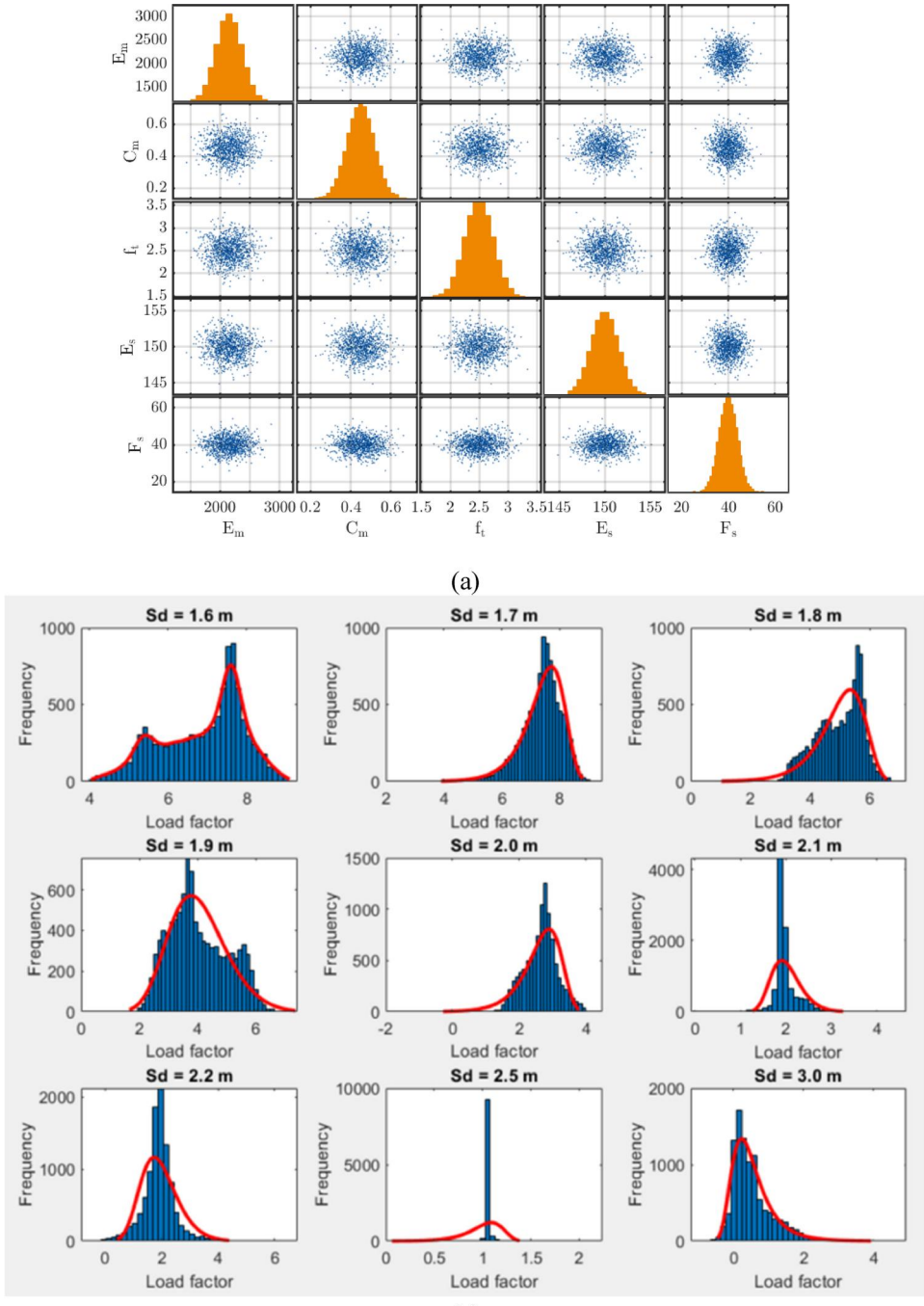

Figure 17. Parameters of the surrogate model: (a) input: MC sample of the selected random variables, and (b) output: Histogram and fitted probabilistic distribution for each scour depth (Sd).

Similar behaviour of the two foundations can be observed when they are subjected to local scour, which was expected due to the symmetry of the bridge. In addition, both fragility curves were generated based on the failure modes described in Section 4, where soil failure does not occur until the scour depth exceeds 2.5 m and the soil under the foundations has a limited bearing capacity.

5.3. Discussion

In the present study, a probabilistic-based methodology was successfully applied to evaluate the scour fragility conditions of a masonry arch bridge. Which employs surrogate modelling techniques to overcome the computational cost associated to the non-linear finite element models. The kriging surrogate model allows to obtain the ultimate load capacity, including the effects of soil-structure interaction, based on the influence of the uncertainties associated to key parameters, selected using a sensitivity analysis.

However, there are some limitations with the adopted methodology, namely regarding the training set of the surrogate model, which may greatly influence the results of the reliability analysis. The limit state should be clearly defined before the definition of the training sample to ensure a

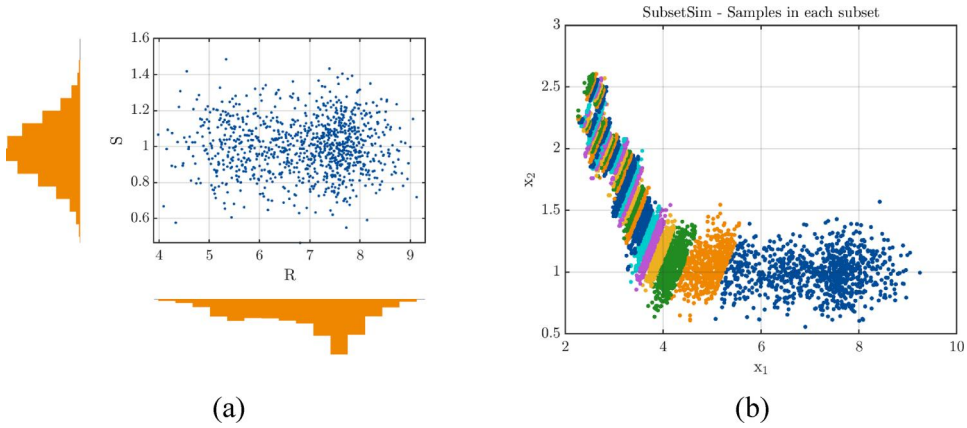

Figure 18. Process to obtain failure probability: (a) starting sampling (model uncertainties are not in the graph); and (b) subset simulation graphical process (where X_1 is S and X_2 is R).

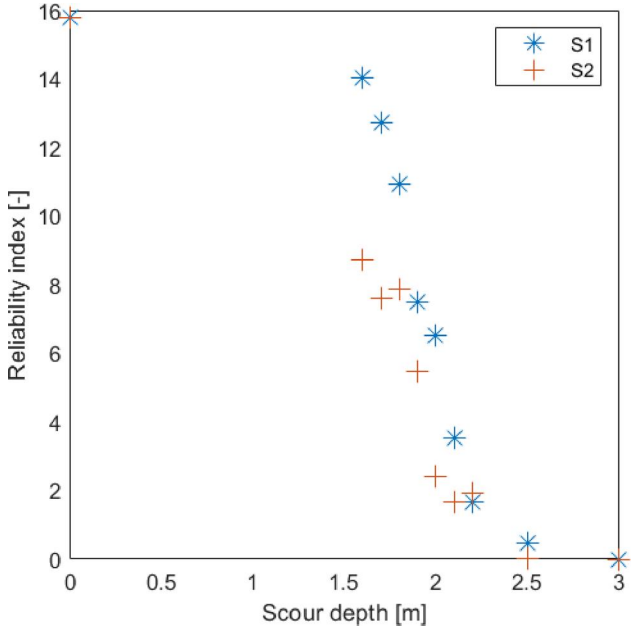

Figure 19. Reliability index of the case study for each scour depth value.

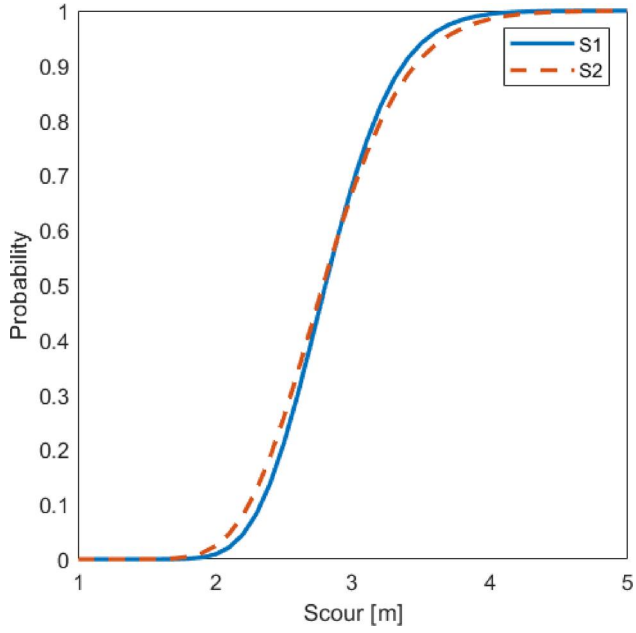

Figure 20. Fragility curve for the two foundations.

reliable result from the surrogate model. However, defining a training sample near this region may carry some challenges since the limit state often appear in regions far from the expected capacity. In the current research, this was addressed by including different intensities of the hazard, i.e. fragility curves based on scour depth, effectively representing different scenarios were the limit state is closer to the expected capacity. Finally, the exploration of different methodologies to define the training sample will be included in future research.

Although the results of this study lead to a better understanding of the scour vulnerability of masonry arch bridges and contribute to the assessment and management of risks associated with scour effects, there are other limitations that should be mentioned. The results from the numerical model are calibrated based on results from non-destructive tests performed on the case study, effectively allowing for the calibration of the model to be based on the linear behaviour of the structure. For this particular case, the available information from the dynamic characterization allowed the calibration of the modulus of elasticity, which was found to have the greatest uncertainty and influence on the dynamic response of the structure. Moreover, the study focuses in the parameter uncertainties from resistance parameters, and uncertainties related to bridge geometry and loading, were not explored but it is advised to include them in future research.

By addressing these limitations and incorporating more comprehensive data and experimental investigations, future research can build on the results of this study and further refine the understanding of how other masonry bridges respond to local scour effects. Although the present methodology has only been applied to one case study, the authors believe that the results indicate that it is transferable to other bridges of similar typology and local condition, providing a deeper understanding of their response to scour effects and can be used to support decision making, resulting in improved safety while reducing maintenance and repair costs. However, it is recommended that further case studies are carried out to further support and validate the

potential of the proposed scour reliability assessment method.

6. Conclusions

The following conclusions can be drawn from the results obtained in this study:

- Finite element modelling provides a good representation of the structure, which, when combined with dynamic calibration, allows for a more detailed response of the structure. However, due to the stochastic nature of the reliability analyses, the computational requirements may be too high. To overcome this, surrogate models with sensitivity analysis provide a more efficient framework for evaluating structures.
- In the sensitivity analysis, the most important parameters for the failure mode are the mechanical parameters used for the constitutive model of weaker soil layers and masonry materials. Therefore, the common parameter is the modulus of elasticity, i.e. stiffness, which is important for soil-structure interaction.
- For the fragility analysis, only the information where soil removal affects the behavior of the structure, and its stability was considered. In other words, for values where the scour depth is below the foundation level. This explains the range in which the fragility curves were defined, i.e. scour depths greater than 1.5 m.
- The scour behavior of the two foundations was not similar. This can be explained by the different geometry of the two piers and the location of the loading during the analysis. However, when the failure mechanism is in the soil, it shows the same behavior due to its symmetry to transfer the load to the foundation.
- With each increase in scour depth, the reliability of the bridge decreased. However, for scour depths less than 1.5 m, the reduction in bearing capacity remained relatively insignificant. It is worth noting that where the majority of the scour depth values were below the foundation level (<1.5 m), the reliability index decreased to levels below the accepted safety limits.

Acknowledgements

This research was carried out at the University of Minho in close collaboration with 'Infraestruturas de Portugal (IP)', the Portuguese Authority responsible for the conservation of bridges. This work was partially funded by: (i) national funds through the FCT - Foundation for Science and Technology, under grant agreements 'PD/BD/143142/2019' attributed to the first author and '2022.09751.BD' attributed to the second author; and (ii) FCT/MCTES through national funds (PIDDAC) under the R&D Unit Institute for Sustainability and Innovation in Structural Engineering (ISISE), under reference UIDB/04029/2020.

Disclosure statement

The authors reported no potential conflict of interest.

References

Ahamed, T., Duan, J. G., & Jo, H. (2021). Flood-fragility analysis of instream bridges–consideration of flow hydraulics, geotechnical uncertainties, and variable scour depth. *Structure and Infrastructure Engineering*, *17*(11), 1494–1507. doi:10.1080/15732479.2020.1815226

Arêde, A., Costa, C., Gomes, A. T., Menezes, J. E., Silva, R., Morais, M., & Gonçalves, R. (2017). Experimental characterization of the mechanical behaviour of components and materials of stone masonry railway bridges. *Construction and Building Materials*, *153*, 663–681. doi:10.1016/j.conbuildmat.2017.07.069

Argyroudis, S. A., & Mitoulis, S. A. (2021). Vulnerability of bridges to individual and multiple hazards-floods and earthquakes. *Reliability Engineering & System Safety*, *210*, 107564. 107564. doi:10.1016/j.ress.2021.107564

Argyroudis, S. A., Mitoulis, S., Winter, M. G., & Kaynia, A. M. (2019). Fragility of transport assets exposed to multiple hazards: State-of-the-art review toward infrastructural resilience. *Reliability Engineering & System Safety*, *191*(December 2018), 106567. doi:10.1016/j.ress.2019.106567

Au, S. K., & Beck, J. L. (2001). Estimation of small failure probabilities in high dimensions by subset simulation. *Probabilistic Engineering Mechanics*, *16*(4), 263–277. doi:10.1016/S0266-8920(01)00019-4

Banerjee, S., & Ganesh Prasad, G. (2013). Seismic risk assessment of reinforced concrete bridges in flood-prone regions. *Structure and Infrastructure Engineering*, *9*(9), 952–968. doi:10.1080/15732479.2011.649292

Baron, E. A. Galvão, N., Docevska, M., Matos, J. C., & Markovski, G. (2023). Application of quality control plan to existing bridges. *Structure and Infrastructure Engineering, 19*(7), 990–1006. doi:10.1080/15732479.2021.1994618

Baron, E. A., Matos, J., Calçada, R., & Gavin, K. (2023). (*Structural damage identification for robustness assessment of railway infrastructure under flood effects*). (Doctoral Thesis). University of MInho.

Bento, A. M., Gomes, A., Viseu, T., Couto, L., & Pêgo, J. P. (2020). Risk-based methodology for scour analysis at bridge foundations. *Engineering Structures*, *223*, 111115. 111115. doi:10.1016/j.engstruct.2020.111115

Brandimarte, L., Paron, P., & Di Baldassarre, G. (2012). Bridge pier scour: A review of processes, measurements and estimates. *Environmental Engineering and Management Journal*, *11*(5), 975–989. doi:10.30638/eemj.2012.121

Conde, B., Matos, J. C., Oliveira, D. V., & Riveiro, B. (2021). Probabilistic-based structural assessment of a historic stone arch bridge. *Structure and Infrastructure Engineering*, *17*(3), 379–391. doi:10.1080/15732479.2020.1752261

Conde, B., Ramos, L. F., Oliveira, D. V., Riveiro, B., & Solla, M. (2017). Structural assessment of masonry arch bridges by combination of non-destructive testing techniques and three-dimensional numerical modelling: Application to Vilanova bridge. *Engineering Structures*, *148*, 621–638. doi:10.1016/j.engstruct.2017.07.011

Cook, W. (2014). (*Bridge Failure Rates, Consequences, and Predictive Trends*). (All Graduate Theses and Dissertations).

Costa, C., Ribeiro, D., Jorge, P., Silva, R., Arêde, A., & Calçada, R. (2014). Avaliação experimental e numérica dos parâmetros modais da ponte ferroviária de Durrães. *JPEE 2014, 5as Jornadas Portuguesas de Engenharia de Estruturas*, 26–28.

Costa, C., Ribeiro, D., Jorge, P., Silva, R., Arêde, A., & Calçada, R. (2016). Calibration of the numerical model of a stone masonry railway bridge based on experimentally identified modal parameters. *Engineering Structures*, *123*, 354–371. doi:10.1016/j.engstruct.2016.05.044

Dearman, W. R. (1995). Description and classification of weathered rocks for engineering purposes: The background to the BS5930: 1981 proposals. *Quarterly Journal of Engineering Geology*, *28*(3), 267–276. doi:10.1144/GSL.QJEGH.1995.028.P3.05

Dong, Y., Frangopol, D. M., & Saydam, D. (2013). Time-variant sustainability assessment of seismically vulnerable bridges subjected to multiple hazards. *Earthquake Engineering & Structural Dynamics*, *42*(10), 1451–1467. doi:10.1002/eqe.2281

dos Santos Adrião, V. (2018). *Modelação numérica da ponte ferroviária em alvenaria de pedra sobre o rio Leça*.

Douben, K. (2006). Characteristics of river floods and flooding: A global overview, 1985–2003. *Irrigation and Drainage*, *55*(S1), S9–S21. doi:10.1002/ird.239

European Committee for Standardization. (2003). *EN 1991-2, Eurocode 1: Actions on structures - Part 2: Traffic loads on bridges*. Belgium: Brussels.

Guimarães, H., Matos, J. C., & Henriques, A. A. (2018). An innovative adaptive sparse response surface method for structural reliability analysis. *Structural Safety*, *73*, 12–28. doi:10.1016/j.strusafe.2018.02.001

Hansen, J. (1970). *A revised and extended formula for bearing capacity*. https://trid.trb.org/view/125129.

Hung, C.-C., & Yau, W.-G. (2017). Vulnerability evaluation of scoured bridges under floods. *Engineering Structures*, *132*, 288–299. doi:10.1016/j.engstruct.2016.11.044

Infraestruturas de Portugal. (2020). *Relatório de inspeção principal global [Global main inspection report]*.

ISRM. (1981). Basic geotechnical description of rock masses. ISRM Commission on the Classification of Rocks and Rock Masses. *Int. J. Rock Mech. Mining Sci. Geom. Abst*, *18*, 85–110.

Jaishi, B., & Ren, W.-X. (2005). Structural finite element model updating using ambient vibration test results. *Journal of Structural Engineering*, *131*(4), 617–628. doi:10.1061/(ASCE)0733-9445(2005)131:4(617)

JCSS. (2006). JCSS probabilistic model code part 3: Resistance models. In Lancet doi:10.1016/S0140-6736(06)69720-1

Khandel, O., & Soliman, M. (2021). Integrated framework for assessment of time-variant flood fragility of bridges using deep learning neural networks. *Journal of Infrastructure Systems*, *27*(1), 4020045. doi:10.1061/(ASCE)IS.1943-555X.0000587

Kim, H., Sim, S.-H., Lee, J., Lee, Y.-J., & Kim, J.-M. (2017). Flood fragility analysis for bridges with multiple failure modes. *Advances in Mechanical Engineering*, *9*(3), 168781401769641. 1687814017696415. doi:10.1177/1687814017696415

Lamb, R., Aspinall, W., Odbert, H., & Wagener, T. (2017). Vulnerability of bridges to scour: Insights from an international expert elicitation workshop. *Natural Hazards and Earth System Sciences*, *17*(8), 1393–1409. doi:10.5194/nhess-17-1393-2017

Lourenço, P. B. (2002). Computations on historic masonry structures. *Progress in Structural Engineering and Materials*, *4*(3), 301–319. doi:10.1002/pse.120

Marelli, S., & Sudret, B. (2014). *UQLab: A Framework for Uncertainty Quantification in MATLAB*. The 2nd International Conference on Vulnerability and Risk Analysis and Management (ICVRAM 2014), 2554–2563. doi:10.1061/9780784413609.257

Matos, J. C., Moreira, V. N., Valente, I. B., Cruz, P. J. S., Neves, L. C., & Galvão, N. (2019). Probabilistic-based assessment of existing steel-concrete composite bridges – Application to Sousa River Bridge. *Engineering Structures*, *181*(December 2018), 95–110. doi:10.1016/j.engstruct.2018.12.006

Melville, B. W., & Coleman, S. E. (2000). *Bridge scour*. Colorado: Water Resources Publication.

Mendoza Cabanzo, C., Santamaría, M., Sousa, H. S., & Matos, J. C. (2022). In-plane fragility and parametric analyses of masonry arch bridges exposed to flood hazard using surrogate modeling techniques. *Applied Sciences*, *12*(4), 1886. doi:10.3390/app12041886

Nelder, J. A., & Wedderburn, R. W. M. (1972). Generalized linear models. *Journal of the Royal Statistical Society. Series A (General)*, *135*(3), 370. doi:10.2307/2344614

NP EN 1990: 2009. (2009). Norma Portuguesa - Eurocódigo 0 - Bases para o projeto de estruturas. *Instituto Português Da Qualidade*, *1999*, 88.

Olofsson, I., Elfgren, L., Bell, B., Paulsson, B., Niederleithinger, E., Sandager Jensen, J., … Bien, J. (2005). Assessment of European railway bridges for future traffic demands and longer lives – EC project "Sustainable Bridges". *Structure and Infrastructure Engineering*, *1*(2), 93–100. doi:10.1080/15732470412331289396

Proske, D. (2018). Comparison of bridge collapse frequencies with failure probabilities Comparison of Bridge Collapse Frequencies with Failure Probabilities. March

Ramos, L. F., Sena-Cruz, J., & Ferreira, R. M. (2011). *Caracterização dinâmica da ponte Luiz Bandeira em Sejães*. 2° Congresso de Segurança e Conservação de Pontes (ASCP2011), 143–152.

Rangel, C. C. (2016). *Evaluación del impacto de las alteraciones climáticas en un puente de concreto preesforzado*. Guimarães, Portugal: Universidade do Minho.

Scozzese, F., Ragni, L., Tubaldi, E., & Gara, F. (2019). Modal properties variation and collapse assessment of masonry arch bridges under scour action. *Engineering Structures*, *199*, 109665. 109665. doi:10.1016/j.engstruct.2019.109665

Shirole, A. M., & Holt, R. C. (1991). Planning for a comprehensive bridge safety assurance program. *Transportation Research Record*, *1290*, 39–50.

Silva, R., Costa, C., & Arede, A. (2018). *Experimental and numerical approaches for calibration of the material parameters used in models of stone masonry railway bridges*. The Fourth International Conference on Railway Technology.

Silva, R., Costa, C., & Arêde, A. (2022). Numerical methodologies for the analysis of stone arch bridges with damage under railway loading. *Structures*, *39*(March), 573–592. doi:10.1016/j.istruc.2022.03.063

Silva, R., Costa, C., Arêde, A., Calçada, R., & Oliveira, D. V. (2019). *Structural analysis of a stone arch bridge under incremental railway static loading*. doi:10.2749/guimaraes.2019.1536

Soares, L., Araújo, A., & Gomes, A. A. (2011). Contexto geográfico do território do Leça. *O Rio Da Memória: Arqueologia Do Território Do Leça*.

TNO DIANA. (2016). User's Manual - Element Library. In *TNO DIANA bv* (Release 10).

Tubaldi, E., Antonopoulos, C., Mitoulis, S. A., Argyroudis, S., Gara, F., Ragni, L., … Pitilakis, D. (2022). Field tests and numerical analysis of the effects of scour on a full-scale soil–foundation–structural system. *Journal of Civil Structural Health Monitoring*, *13*(8), 1461–1481. doi:10.1007/s13349-022-00608-x

Tubaldi, E., Macorini, L., & Izzuddin, B. A. (2018). Three-dimensional mesoscale modelling of multi-span masonry arch bridges subjected to scour. *Engineering Structures*, *165*, 486–500. doi:10.1016/j.engstruct.2018.03.031

Tubaldi, E., Macorini, L., & Izzuddin, B. A. (2020). Identification of critical mechanical parameters for advanced analysis of masonry arch bridges. *Structure and Infrastructure Engineering*, *16*(2), 328–345. doi:10.1080/15732479.2019.1655071

Wardhana, K., Hadipriono, F. C., & Asce, F. (2003). *Analysis of Recent Bridge Failures in the United States*. *August*, 144–150. doi:10.1061/(ASCE)0887-3828(2003)17:3(144)

Xiong, W., Cai, C. S., Zhang, R., Shi, H., & Xu, C. (2023). Review of hydraulic bridge failures: Historical statistic analysis, failure modes, and prediction methods. *Journal of Bridge Engineering*, *28*(4), 03123001. doi:10.1061/JBENF2.BEENG-5763

Yang, D. Y., & Frangopol, D. M. (2018). Risk-informed bridge ranking at project and network levels. *Journal of Infrastructure Systems*, *24*(3), 4018018. doi:10.1061/(ASCE)IS.1943-555X.0000430

Yang, F., Zheng, X.-C., Zhao, L.-H., & Tan, Y.-G. (2016). Ultimate bearing capacity of a strip footing placed on sand with a rigid basement. *Computers and Geotechnics*, *77*, 115–119. doi:10.1016/j.compgeo.2016.04.009

Yilmaz, T., Banerjee, S., & Johnson, P. A. (2018). Uncertainty in risk of highway bridges assessed for integrated seismic and flood hazards. *Structure and Infrastructure Engineering*, *14*(9), 1182–1196. doi:10.1080/15732479.2017.1402065

Zampieri, P., Faleschini, F., Zanini, M. A., & Simoncello, N. (2018). Collapse mechanisms of masonry arches with settled springing. *Engineering Structures*, *156*(vember 2017), 363–374. doi:10.1016/j.engstruct.2017.11.048

Zampieri, P., Zanini, M. A., Faleschini, F., Hofer, L., & Pellegrino, C. (2017). Failure analysis of masonry arch bridges subject to local pier scour. *Engineering Failure Analysis*, *79*, 371–384. doi:10.1016/j.engfailanal.2017.05.028